JOURNAL OF AIRCRAFT
Vol. 42, No. 2, March–April 2005

Simulation of Aircraft Response to Control Surface Deflection Using Unstructured Dynamic Grids

Mitsuhiro Murayama,* Fumiya Togashi,* Kazuhiro Nakahashi,† Kisa Matsushima,‡ and Takuma Kato§
Tohoku University, Sendai 980-8579, Japan

The computational techniques required for flight-test simulation in which the deflection angle of a tail wing is changed are discussed. To treat the computational grid for a moving control surface, an unstructured dynamic mesh method with surface-grid movement is used. This method is applied to the numerical simulation of the control-surface response for an experimental supersonic airplane at the National Aerospace Laboratory of Japan. Its high capability is demonstrated in both steady and unsteady simulations.

Introduction

In the past 30 years, with the rapid growth of computational resources, computational fluid dynamics (CFD) has achieved significant progress and is considered to be very close to maturation in flow computation around airplanes under designed conditions. The next target of CFD is numerical simulation of maneuvered airplanes, including their response to control surface deflection and aeroelasticity. The precise prediction of flow characteristics when an airplane is being maneuvered is important for design and for design analysis. One of the most important issues in maneuvering is stability control of the longitudinal motion of an airplane, such as trim. For trim, we need to know the aerodynamic forces operating at many deflection angles of a control surface under various flight conditions. Usually, trim is considered for static stability control. Furthermore, trim is important for dynamic stability control, for which we need to know the dynamic response of the aerodynamic forces to unsteady control-surface deflection. However, this type of experiment is extremely difficult to conduct in a wind tunnel. Thus, CFD holds great promise for solution of this type of dynamic-response problem as well as for clarification of the static response. Recently, the concept of movement of the entire tail wing as a control surface was adopted for high-speed commercial transport, such as the Airbus A3xx series and an experimental supersonic airplane of Japan. For the simulation of such response problems, a computational method for treating geometrically complex airplanes is required. In addition, movement of the control surface and airplane must be taken into consideration.

In this paper, flow computations around moving and deforming bodies are discussed. To treat these problems numerically, the existing grid must be moved, accompanied by movement and deformation of the body. For the simulation of flow with moving rigid bodies, the overset unstructured grid technique,[1–3] which uses several unstructured grids to cover the flow field of moving bodies, is very useful. The rigid flapping motion of a hornet was solved by this method and this method showed reasonable results.[3] On the other hand, for the simulation of flow of deforming bodies or the treatment of changes of the intersection of the wing and fuselage, the dynamic mesh method is preferable.

Received 1 January 2003; accepted for publication 7 October 2003.

*Graduate Student, Department of Aeronautics and Space Engineering, Aramaki-Aza-Aoba 01.
†Professor, Department of Aeronautics and Space Engineering, Aramaki-Aza-Aoba 01. Associate Fellow AIAA.
‡Associate Professor, Department of Aeronautics and Space Engineering, Aramaki-Aza-Aoba 01. Member AIAA.
§Research Associate, Department of Aeronautics and Space Engineering, Aramaki-Aza-Aoba 01. Member AIAA.

One requirement of the dynamic mesh method is robustness, which should not create ill-conditioned cells during movement of the mesh. Several methods for dynamic mesh have been developed and have shown good results for problems with small-amplitude oscillation and deformation.[4–9] The most common approach when dynamic meshes are employed is to use the linear tension spring analogy.[4] With this approach, however, the cell shape cannot be controlled, often resulting in the formation of ill-conditioned cells for large movements. To counteract this, in our previous work,[10] each tetrahedron cell shape in the grid, such as internal angles of triangular faces and angles between two faces that constitute the cell, is controlled in order not to generate squashed, invalid cells. Results showed improvement of robustness without much loss of CPU time.

In computing the maneuver of an aircraft in response to control-surface deflection, we encounter another difficulty, namely, the treatment of the computational grid for the moving control surface, for example, a tail wing. Because of the change in location of a tail wing on a fuselage surface, the surface grid of the tail wing–fuselage juncture should be changed. In general moving-body problems, the dynamic mesh method of the three-dimensional volume grid is required to treat the body movement. On the other hand, to treat the change of the deflection angle of the control surface, surface grid points of the fuselage also have to be moved while the original curved surface of the fuselage is maintained, due to the change of the intersection. However, it is difficult to directly move the surface grid points along the curved surface without changing the original topology and geometry. In this paper, a surface-mapping moving-grid method[10] developed by the present authors is applied. A partially cut out three-dimensional surface grid is mapped onto a two-dimensional parameter domain. The moving-grid method is then applied to the parameter plane. The moved grid is then transformed back onto the three-dimensional surface. By the use of this method, the surface grid can be also moved along the curved surface.

The final goal of this study is to conduct an unsteady simulation of the dynamic flight control of an aircraft during maneuvers. In this paper, the computational techniques required for the flight-test simulation are discussed. In addition, these techniques are applied to the numerical simulation of control-surface response for an experimental supersonic airplane at the National Aerospace Laboratory (NAL) of Japan.

Mesh Point Movement Method

In this study, the unstructured dynamic mesh method used in Ref. 10, which is based on the linear tension spring analogy method,[4] is employed. Suppose an unstructured mesh system is composed of tetrahedral elements. Figure 1 shows one tetrahedral element. In this method, each edge of an element is modeled as a linear tension spring. The forces $\boldsymbol{F}_{\text{spring}\,ij}$ are generated by these springs at each vertex by the mesh-point movement,

$$\boldsymbol{F}_{\text{spring}\,ij} = k_{\text{spring}\,ij}\,\Delta\boldsymbol{x}_{ij} \tag{1}$$

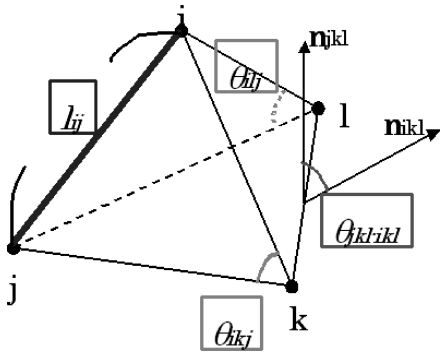

Fig. 1 Determination of spring coefficients for a tetrahedron.

where $k_{\text{spring}\,ij}$ is the spring stiffness coefficient at edge ε_{ij} and $\boldsymbol{\Delta x}_{ij}$ is the displacement. The static equilibrium equations, Eq. (2), of these forces are solved iteratively at each interior node and the displacements in the x, y, and z directions are determined:

$$\sum_{f \in \varepsilon_{ij}} \boldsymbol{F}_{\text{spring}\,ij} = 0 \tag{2}$$

Here, grid points on the outer boundary of the mesh are fixed and the displacement on the body surface is given as the initial condition. By the use of edge length l_{ij} as the spring stiffness described by Eq. (3), the method can prevent one vertex from colliding with the other:

$$k_{\text{spring}\,ij} = 1/l_{ij} \tag{3}$$

However, the method does not prevent a vertex from crossing edges and faces. In the problems with relatively greater motion, therefore, the method can generate invalid elements. To prevent this, the geometry of the elements should be considered.

In this study, three-dimensional grids composed of tetrahedras are assumed, as shown in Fig. 1. To prevent the faces from squashing, the internal angles of triangles, which share edge ε_{ij}, are considered. Moreover, to prevent the tetrahedron volume from becoming zero or negative, the angles between two faces, $\theta_{jkl-ikl}$, are considered. The spring coefficients at edge ε_{ij} are determined by using these angles as follows:

$$k_{\text{angle}\,ij} = \sum \frac{1}{\sin^2 \theta} \tag{4}$$

$$k_{ij} = k_{\text{spring}\,ij} + k_{\text{angle}\,ij} \tag{5}$$

Because $k_{\text{angle}\,ij} \to \infty$ when $\theta \to \pi$ or 0, the spring prevents the cells from squashing and having zero or negative area.

In addition, when the method is applied to practical fluid problems, the wall distance function $f_d \propto 1/d$ is multiplied by the spring stiffness coefficients to suppress the deformation of the grid near the wall and to keep its original clean shape.

Surface Grid Movement

For simulation of an airplane's response to control-surface deflection, the surface grids on the fuselage near the fuselage–control wing juncture have to be moved according to the movement of the control wing. However, to move the surface grids while maintaining the original curved surface plane is not easy, because no straightforward information is provided about the original surface curvature. There is only information on discrete grid point coordinates. In other words, it is difficult to directly move the surface grid points along the curved surface in a proper manner.

Here, the surface-mapping moving-grid method[10] developed by the present authors is used, in which mapping of the surface component onto a two-dimensional parameter domain is applied. This idea is similar to the algorithm for generating unstructured surface grids.[11] A three-dimensional surface grid region is partially cut out and mapped onto a two-dimensional parameter domain as shown in Fig. 2. The moving grid method discussed in the previous section is then applied to the parameter domain. The moved grid is transformed back to the three-dimensional surface. By the use of this method, the tail wing can be moved smoothly.

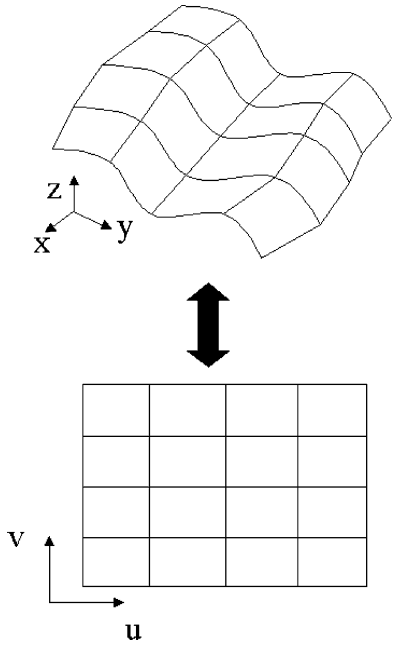

Fig. 2 Mapping of surface.

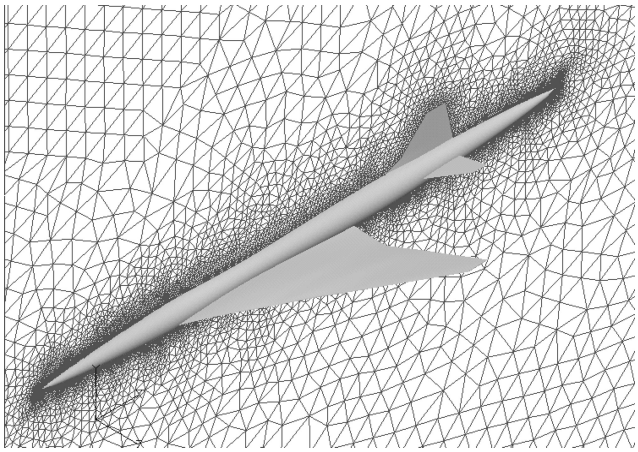

Fig. 3 Computational grid of an experimental supersonic airplane of the National Aerospace Laboratory of Japan.

Flow Solver

The original unstructured surface grid and the tetrahedral volume grid are generated by the method described in Refs. 12–14. The Euler equations are solved considering the grid movement. The Harten–Lax–van Leer–Einfeldt–Wada Riemann solver[15] is used for the numerical flux computations. Second-order spatial accuracy is realized by a linear reconstruction of the primitive variables. The lower/upper symmetric Gauss–Seidel implicit method for the unstructured grid[16] is used for the time integration.

Results

The proposed method combined with the three-dimensional dynamic mesh and surface dynamic mesh was applied to the numerical simulation of the longitudinal stability control of the experimental supersonic airplane shown in Fig. 3. This is a real airplane that the NAL is currently working on. The project is developing experimental supersonic airplanes to conduct a basic study for the supersonic transport of the next generation. In this airplane, a horizontal tail

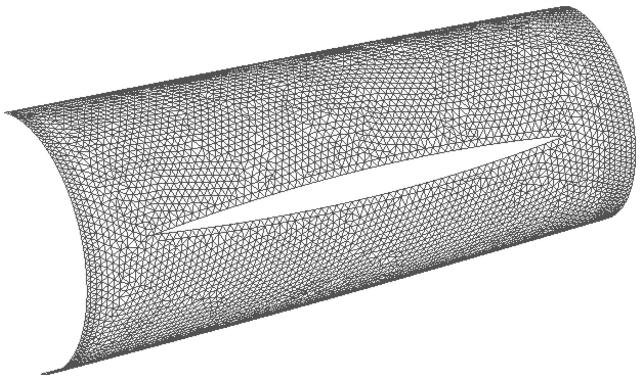

Fig. 4 Surface grid cut out near the horizontal tail wing.

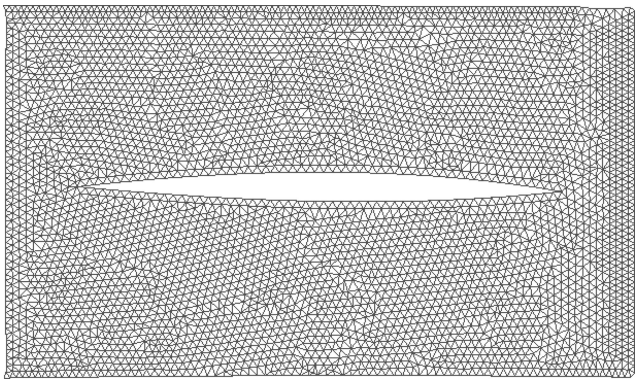

Fig. 5 Grid transformed onto the two-dimensional parameter domain.

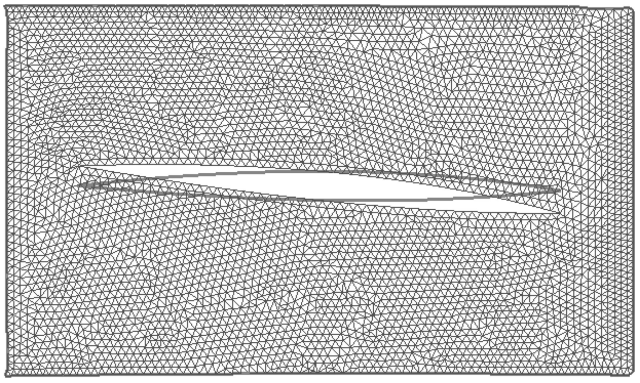

Fig. 6 Grid moved onto a parameter domain.

wing that moves in its entirety is adopted as the control surface, which controls the longitudinal stability. Figure 3 shows the computational grid of the experimental airplane. The total number of grid points is about 0.3 million.

The processes of surface grid movement due to the change of the deflection angle of the horizontal tail wing are shown in Figs. 4–7. The horizontal tail wing is moved, so that the deflection angle is changed from 0 to 5 deg. First, the junction between the fuselage and tail surface is determined and a three-dimensional unstructured surface grid region near the junction is cut out as shown in Fig. 4. Then a fine regular patch grid along the curved fuselage surface is constructed and the linear interpolation information between the surface grid and the patch grid is formulated. The transformation of the grids onto a two-dimensional parameter domain is shown in Fig. 5. The regular patch grid is easily transformed onto such a domain. The three-dimensional unstructured surface grid is then transformed onto the parameter domain based on the formulated interpolation information. The moving grid method is then applied to the parameter plane shown in Fig. 6. Again, interpolation information

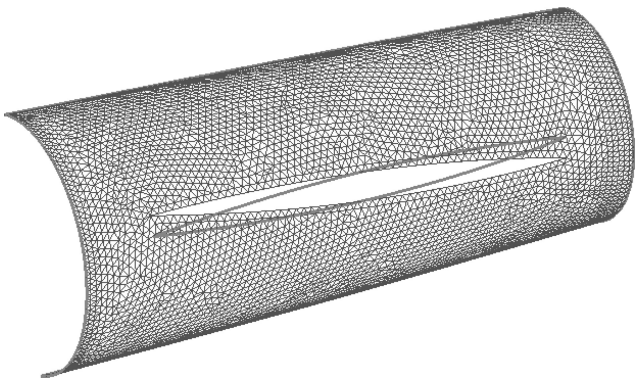

Fig. 7 Grid transformed back onto the three-dimensional surface.

is formulated after the grid has been moved and the moved grid is then transformed back onto the three-dimensional surface as shown in Fig. 7. Finally, the tetrahedral volume grid is moved according to the surface grid movement using the method described in the previous section.

In changing the deflection angle of the horizontal tail wing, the surface configuration of the airplane must usually be redefined using CAD, etc., and the surface grid must be regenerated. Then the computational volume grid is newly generated and computation is performed. The process of redefinition of the surface configuration and surface and volume grid generation is a time-consuming task, which takes about 2 h by a skilled engineer in this case. By the use of the surface grid movement method and dynamic mesh method, this process can be easily and automatically conducted in only a few minutes. Hence, with the proposed method, the aerodynamic forces resulting from the change of both the angle of attack and the deflection angle of the horizontal tail wing can be estimated efficiently, and unsteady analysis can also be conducted without much cost.

Steady State Analysis

Euler computations were performed with changes in the angle of attack and the deflection angle of the horizontal tail wing. Freestream Mach numbers M_∞ are 2.0 and 0.95. Figures 8 and 9 show the contours of the Mach numbers. In Figs. 8a and 9a, the angle of attack α is 0 deg and the deflection angle of the horizontal tail wing β is 0 deg at each Mach number. Figures 8b and 9b show the results at $\alpha = 4$ deg and $\beta = -5$ deg. In Fig. 9a at $M_\infty = 0.95$, shock waves can be seen on the main wing and the horizontal tail wing. In the case $M_\infty = 0.95$, the effects due to the change of α and β are much greater than in the case $M_\infty = 2.0$. The strength of the shock waves on the main wing is greatly intensified. In particular, a new shock wave is generated under the tail wing by the change of the deflection angle of the tail wing.

Variations of the lift coefficients (C_L) and pitching moment coefficients (C_M) with the angle of attack are shown in Fig. 10. The experimental results are provided courtesy of the aerodynamic group of NAL's scaled experimental SST project. As for C_L and C_M at $M_\infty = 2.0$, computational results show good agreement with experimental results except for at higher angles of attack, as shown in Figs. 10a and 10b. At higher angles of attack, however, the differences become larger. The gradient of C_L vs angle of attack (C_L–α) in the computational results is steeper than that in the experimental results and the difference is 8%. However, the gradient of C_M vs angle of attack (C_M–α) of the experimental results is steeper than that of the computational results and the difference is 14.5%. The same tendency can be seen in other computational results at the third SST–CFD Workshop, held in December 2001, discussed in Ref. 17. Figure 10c shows C_M vs C_L plots (C_M–C_L). In Fig. 10c, the computational results show better agreement with the experimental results and the difference of the gradient is only 6%.

Figure 11 shows C_L and C_M by the deflection angle of the horizontal tail wing (C_L–β and C_M–β) and C_M–C_L plots. In the experiments, C_L and C_M have been measured only at the deflection angles of -10, 0, and 10 deg. The data at other deflection angles

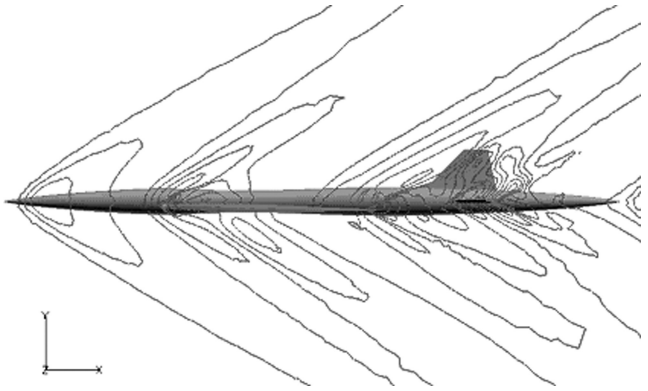

a) $\alpha = 0$ and $\beta = 0$ deg

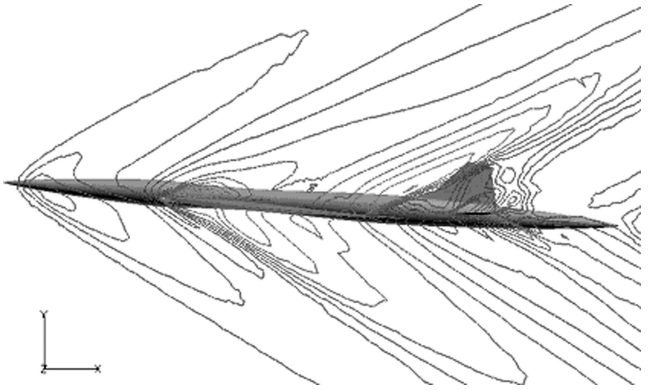

b) $\alpha = 4$ and $\beta = -5$ deg

Fig. 8 Contours of Mach number ($M_\infty = 2.0$): α angle of attack, β deflection angle of the tail wing.

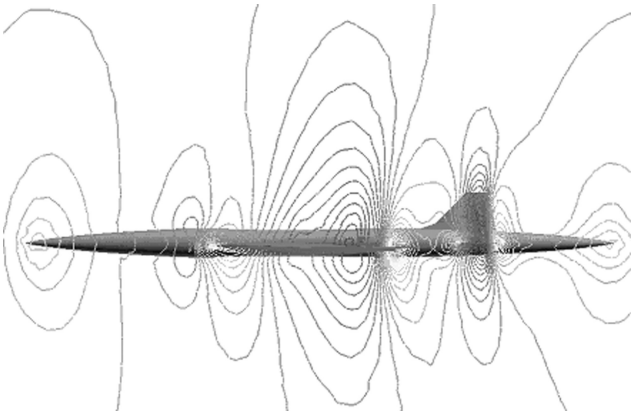

a) $\alpha = 0$ and $\beta = 0$ deg

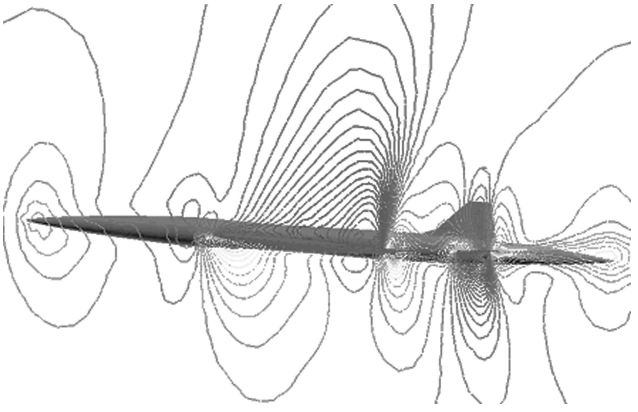

b) $\alpha = 4$ and $\beta = -5$ deg

Fig. 9 Contours of Mach number ($M_\infty = 0.95$): α angle of attack, β deflection angle of the tail wing.

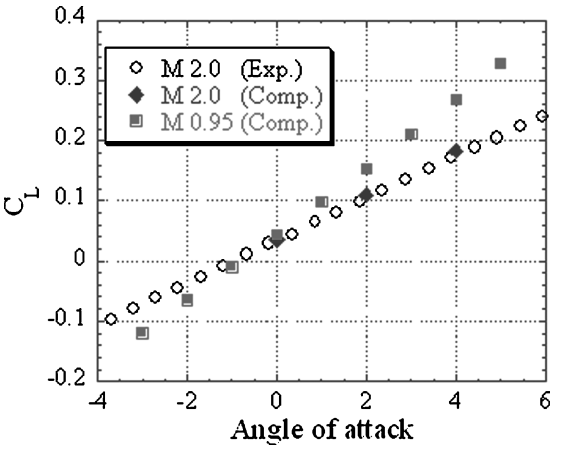

a) Lift coefficients

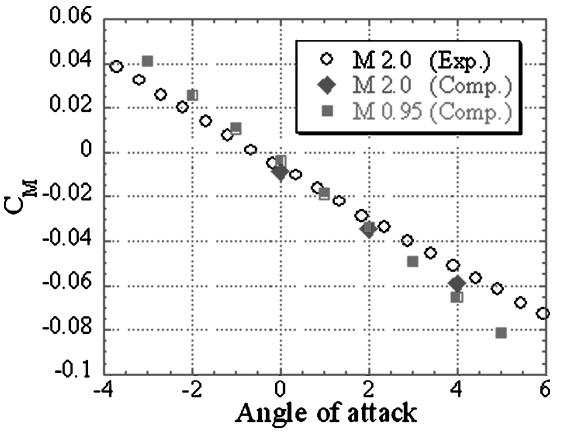

b) Pitching moment coefficients

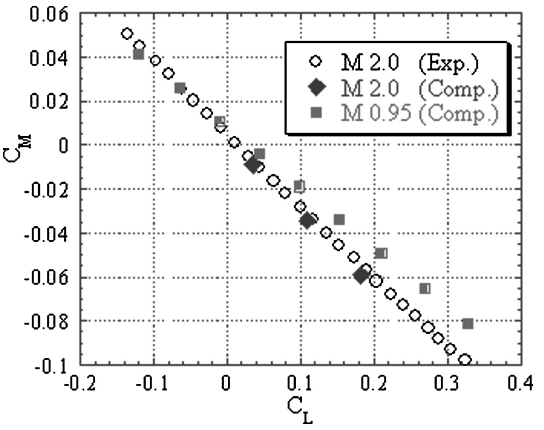

c) Pitching moment coefficients versus lift coefficients

Fig. 10 Variations of the lift coefficients and pitching moment coefficients due to the angle of attack of the wing–fuselage (deflection angle of the horizontal tail wing is zero).

are linearly interpolated from the three points. The computational results at various deflection angles of the horizontal tail wing agree with the experimental results well. The differences of gradients of C_L–β and C_M–β are 10% and 8%. The difference of the gradient of C_M–C_L is 2%. The validity of using the dynamic mesh method for hybrid unstructured meshes is apparent.

From Fig. 11, it can be seen that the aerodynamic forces are linearly affected by the change of the deflection angle of the tail wing at both of the Mach numbers. As for C_L and C_M at these Mach numbers, the assumption of linear interpolation using the three points is proven to be valid. Compared with the results at $M_\infty = 2.0$

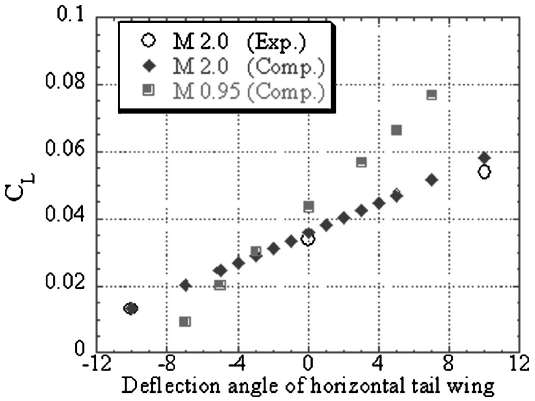

a) Lift coefficients

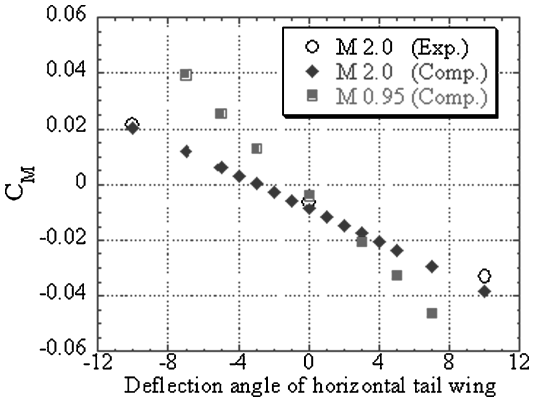

b) Pitching moment coefficients

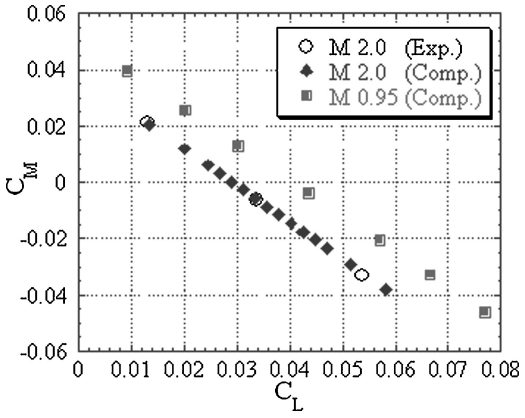

c) Pitching moment coefficients versus lift coefficients

Fig. 11 Variations of the lift coefficients and pitching moment coefficients due to the deflection angle of the horizontal tail wing (angle of attack is zero).

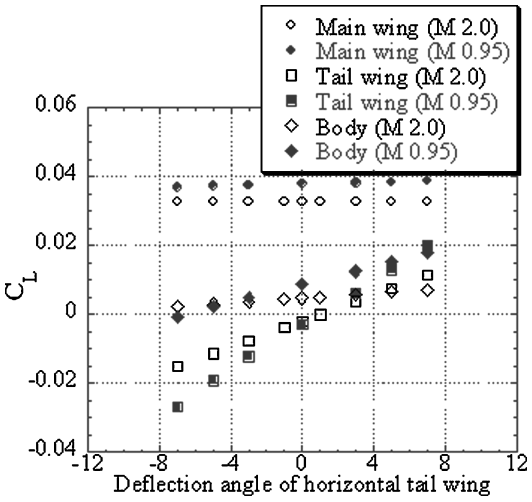

a) Lift coefficients

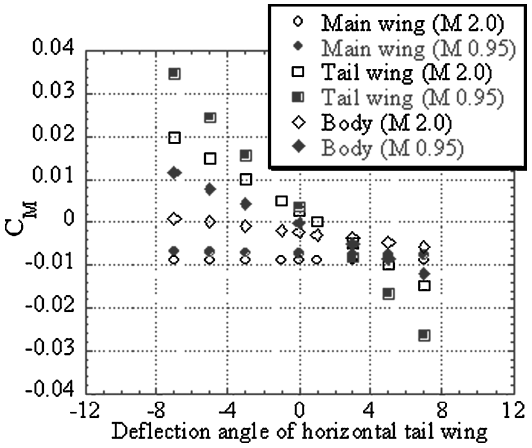

b) Pitching moment coefficients

Fig. 12 Variations of the lift coefficients and pitching moment coefficients due to the deflection angle of the horizontal tail wing at each part (angle of attack is zero).

and 0.95 in Fig. 11, the variation of the aerodynamic coefficients at $M_\infty = 0.95$ is much larger.

The variations of C_L–β and C_M–β, which are separated as to part, i.e., main wing, tail wing, and fuselage, are shown in Fig. 12. The coefficients of the main wing are not much affected by the deflection angle even at $M_\infty = 0.95$. At $M_\infty = 0.95$, the variations at the tail wing and fuselage are much larger. In the case of $M_\infty = 0.95$, the location and strength of the shock waves on the tail wing are greatly changed by the deflection angle. The shock waves on the tail wing affect the aerodynamic forces on the fuselage. Therefore, it can be seen that the total variations of the coefficients at $M_\infty = 0.95$ are larger than those at $M_\infty = 2.0$.

Figure 13 shows the variation of C_L–β at some constant angles of attack. It can be seen that the variation curves at any angle of attack have nearly the same tendency though their levels are different.

Unsteady State Analysis

Computational results of the unsteady response of the airplane to the deflection angle of the horizontal tail wing are shown here. Equations of motion with regard to the airplane are solved at each computational time step with changes of the deflection angle of the tail wing. The freestream Mach number M_∞ is 2.0. The initial angle of attack of the wing–fuselage is 2.0 deg. First, steady Euler computation is performed at the angle of attack. Then the horizontal tail wing is moved, so that the deflection angle is changed from 0.0 to −3.0 deg at 1200 time steps.

Figure 14 shows the contours of the Mach number. It can be seen that the angle of attack of the wing–fuselage is increased according to the change of the deflection angle of the tail wing. Figure 15 shows the history of C_M around the center of gravity of the airplane and C_L. Although C_M was fluctuant at first, C_M had positive values because of the movement of the tail wing. As the deflection angle of the tail wing is decreased from 0.0 deg, the lift of the tail wing is decreased and the total pitching moment is increased. The nose-up movement of the airplane is caused by this moment and C_L becomes larger with the increase of the angle of attack of the wing–fuselage. This aerodynamic movement of the wing–fuselage is reasonable. Although the accuracy of these results should be investigated carefully, these results show that efficient simulation of dynamic stability control is feasible by the methods herein presented.

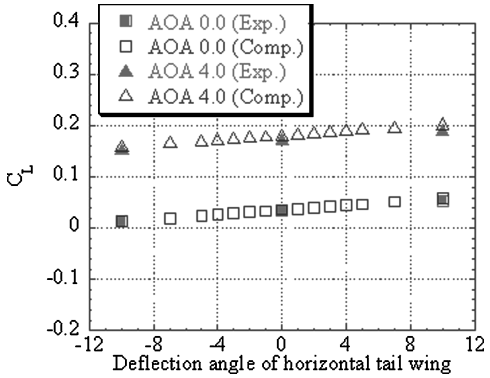

a) $M_\infty = 2.0$

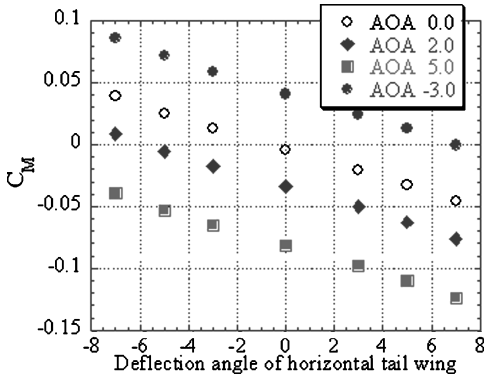

b) $M_\infty = 0.95$

Fig. 13 Variations of the pitching moment coefficients due to the deflection angle of the horizontal tail wing at some constant angles of attack.

Conclusions

The computational techniques required for flight simulation with change of the deflection angle of a tail wing have been herein discussed. By the use of a three-dimensional unstructured dynamic mesh method with surface grid movement, the treatment of the computational grid for a moving control surface could be realized.

The technique was applied to the numerical simulation of control-surface response for an experimental supersonic airplane. Numerical simulation of the static longitudinal stability control could be easily conducted by this method. The validity was proved by comparison with experimental data. Additionally, the computational results at supersonic and transonic speed were compared and the differences of the flow characteristics between the two were estimated.

Moreover, computation of the unsteady response of the airplane to the change of the deflection angle of the horizontal tail wing was conducted. By means of unsteady simulation, it was shown that the method has potential for dynamic flight control simulation.

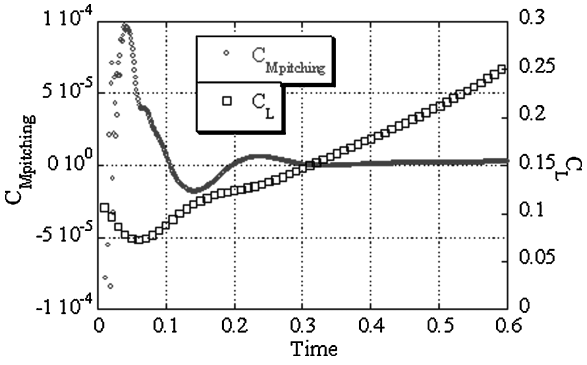

Fig. 15 Time history of the pitching moment and lift coefficients.

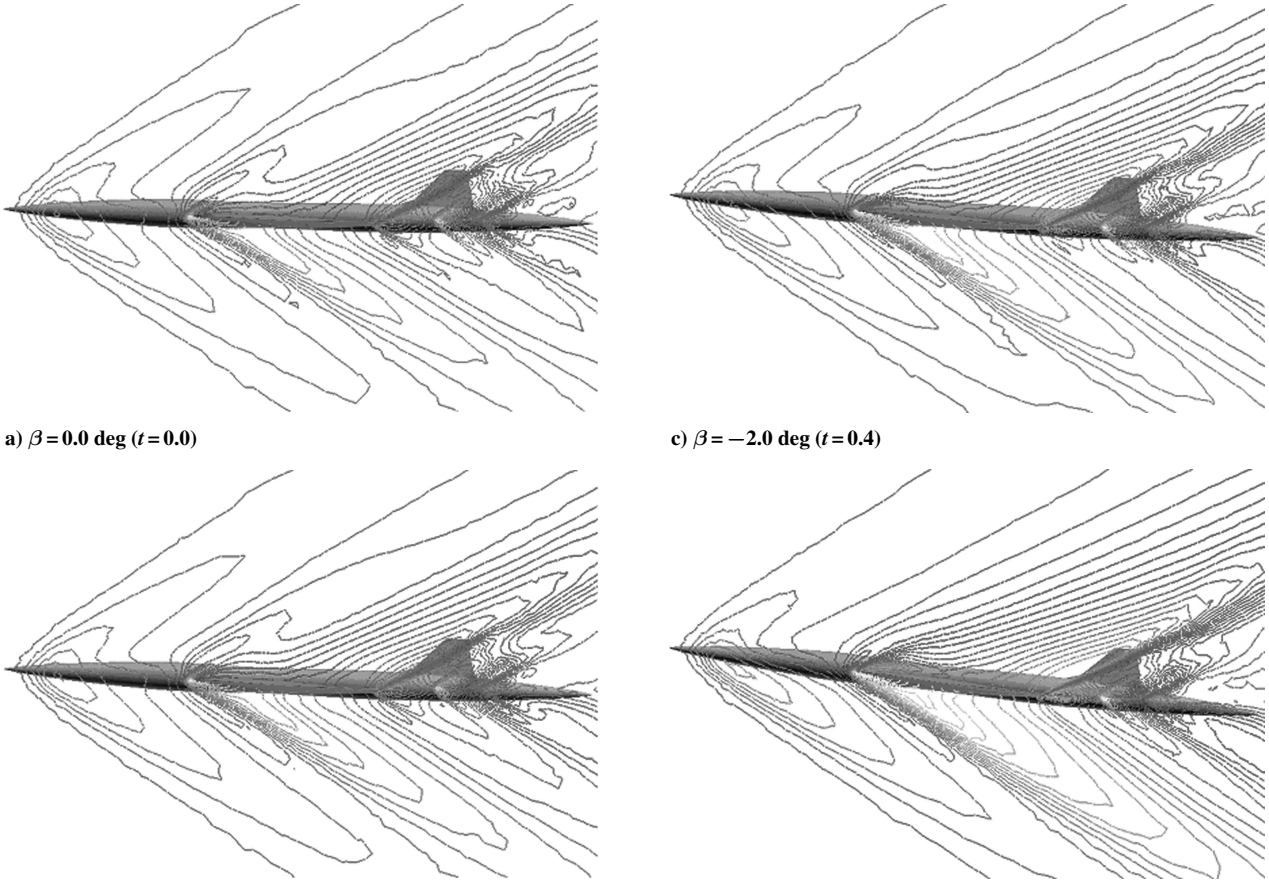

a) $\beta = 0.0$ deg ($t = 0.0$)

c) $\beta = -2.0$ deg ($t = 0.4$)

b) $\beta = -1.0$ deg ($t = 0.2$)

d) $\beta = -3.0$ deg ($t = 0.6$)

Fig. 14 Unsteady computational results: contours of Mach number ($M_\infty = 2.0$).

Acknowledgments

The authors thank the Aerodynamic Design Group, Next Generation Supersonic Transport Project Center, National Aerospace Laboratory of Japan, for providing us with geometric data on the airplane and experimental data. We also thank Y. Ito and T. Fujita, graduate students at Tohoku University, for their help in generating the STL data and unstructured surface grid data.

References

[1]Nakahashi, K., Togashi, F., and Sharov, D., "Intergrid-Boundary Definition Method for Overset Unstructured Grid Approach," *AIAA Journal*, Vol. 38, No. 11, 2000, pp. 2077–2084.

[2]Togashi, F., Nakahashi, K., Ito, Y., Shinbo, Y., and Iwamiya, T., "Flow Simulation of NAL Experimental Supersonic Airplane/Booster Separation Using Overset Unstructured Grids," *Computers and Fluids*, Vol. 30, 2001, pp. 673–688.

[3]Togashi, F., Ito, Y., Murayama, M., Nakahashi, K., and Kato, T., "Flow Simulation of Flapping Wings of an Insect Using Overset Unstructured Grids," AIAA Paper 2001-2619, 2001.

[4]Batina, J. T., "Unsteady Euler Algorithm with Unstructured Dynamic Mesh for Complex Aircraft Aerodynamic Analysis," *AIAA Journal*, Vol. 29, No. 3, 1991, pp. 327–333.

[5]Venkatakrishnan, V., and Mavriplis, D. J., "Implicit Method for the Computation of Unsteady Flows on Unstructured Grids," AIAA Paper 95-1705, 1995.

[6]Löhner, R., Yang, C., Baum, J. D., Luo, H., Pelessone, D., and Charman, C., "The Numerical Simulation of Strongly Unsteady Flows with Hundreds of Moving Bodies," *International Journal for Numerical Methods in Fluids*, Vol. 31, 1999, pp. 113–120.

[7]Tezduyar, T. E., "Finite Element Methods for Flow Problems with Moving Boundaries and Interfaces," *Archives of Computational Methods in Engineering*, Vol. 8, No. 2, 2001, pp. 83–130.

[8]Farhat, C., Degand, C., Koobus, B., and Lesoinne, M., "An Improved Method of Spring Analogy for Dynamic Unstructured Fluid Meshes," AIAA Paper 98-2070, 1998.

[9]Zeng, D., and Ethier C. R., "A Semi-Torsional Spring Analogy Model for Updating Unstructured Meshes," *Proceedings of 9th Annual Conference of the CFD Society of Canada*, 2001.

[10]Murayama, M., Nakahashi, K., and Matsushima, K., "Unstructured Dynamic Mesh for Large Movement and Deformation," AIAA Paper 2002-0122, 2002.

[11]Morgan, K., Peraire, J., and Peiro, J., "Unstructured Grid Methods for Compressible Flows," AGARD-R-787, 1992.

[12]Ito, Y., and Nakahashi, K., "Direct Surface Triangulation Using Stereolithography Data," *AIAA Journal*, Vol. 40, No. 3, 2002, pp. 490–496.

[13]Ito, Y., and Nakahashi, K., "Surface Triangulation for Polygonal Models Based on CAD Data," *International Journal for Numerical Methods in Fluids*, Vol. 39, No. 1, 2002, pp. 75–96.

[14]Sharov, D., and Nakahashi, K., "Hybrid Prismatic/Tetrahedral Grid Generation for Viscous Flow Applications," *AIAA Journal*, Vol. 36, No. 2, 1998, pp. 157–162.

[15]Obayashi, S., and Guruswamy, G. P., "Convergence Acceleration of an Aeroelastic Navier–Stokes Solver," AIAA Paper 94-2268, 1994.

[16]Sharov, D., and Nakahashi, K., "Reordering of Hybrid Unstructured Grids for Lower–Upper Symmetric Gauss–Seidel Computations," *AIAA Journal*, Vol. 36, No. 3, 1998, pp. 484–486.

[17]Takaki, R., Suzuki, N., and Yoshida, K., "Mutual Validation between EFD/CFD for Supersonic Flow around NEXST-1," Proceedings of 24th ICAS Congress (to be published).